Surface & Coatings Technology 484 (2024) 130849

Contents lists available at ScienceDirect

Surface & Coatings Technology

journal homepage: www.elsevier.com/locate/surfcoat

Full length article

Laser assisted electrodeposition of binary metallic alloys from water-based electrolytes: The case of palladium-platinum

Roberto Bernasconi [a,*], Dario Crimella [b], Ali Gökhan Demir [b], Barbara Previtali [b], Luca Magagnin [a]

[a] Dipartimento di Chimica, Materiali e Ingegneria Chimica "Giulio Natta", Politecnico di Milano, Via Mancinelli 7, 20131 Milano, Italy
[b] Dipartimento di Meccanica, Politecnico di Milano, Via La Masa 1, 20156 Milano, Italy

ARTICLE INFO

Keywords:
Laser
Electrodeposition
Alloys
Platinum-palladium

ABSTRACT

The present work investigates the applicability of laser assisted electrodeposition (LAE) to the plating of binary metallic alloys from aqueous solutions and in absence of any external polarization. PdPt was chosen as prototypical system and the deposition was carried out from phosphate-based electrolytes. The effect of electrolyte formulation and laser parameters on the composition, thickness and physical properties of the alloys was studied. In order to provide more insight on the LAE deposition process of alloys, the electrochemical properties of the electrolytes employed were correlated with the properties of the materials obtained. In analogy with standard alloy plating processes, a clear link between the currents observed for the reduction of the two single metals and the composition/thickness of the coated PdPt layers could be established. Compositionally tunable and continuous PdPt coatings were obtained and their chemical, morphological and mechanical properties were determined. Finally, the possibility to selectively deposit the PdPt alloy was demonstrated by patterning a complex figure.

1. Introduction

The applicability of lasers to electrochemistry has become a relevant field of research during the last few decades. Thanks to their ability to deliver a high power density, lasers can be employed to selectively trigger or enhance a variety of electrochemical reactions. For example, they can be used for electrochemistry-assisted laser ablation [1] or for the controlled synthesis of chemical species [2,3]. Lasers can be employed to locally increase electrochemical etching processes, allowing a technique known as laser assisted electrochemical machining (LAECM) [4]. In addition, lasers can also be used to selectively catalyze electrochemical reactions. The most relevant example is electroless deposition, which can be activated by directly patterning catalytic sites on a substrate [5–9] or by locally altering the surface in order to favor the adsorption of activating ions [10–12].

Lasers can also be used to directly promote the deposition of metals and alloys. This can be accomplished following two approaches: laser enhanced electrodeposition (LEE) and laser assisted electrodeposition (LAE). LEE employs a laser to locally reduce metallic ions on a substrate that is polarized using an external source of power [13]. Such polarization is not high enough to start reduction alone and the laser simply provides the energy difference required. In this way, plating takes place only in correspondence of the laser spot, offering thus the possibility to selectively deposit the metal or the alloy. The requirement of external polarization, however, implies the presence of an anode, immersed in the electrolyte together with the substrate (which works as the cathode). Polarization considerably reduces the energy barrier that the laser must overcome to trigger deposition, but it also poses significant limitations due to the necessity to electrically connect the substrate with the external generator. LEE has been exploited to deposit a significant selection of pure metals: Cu [13–16], Au [16,17], Ni [15,16] and Zn [18]. In addition, also the deposition of alloys has been demonstrated: NiFe [19], NiP [20], NiFeP [21,22] and ZnNiMo [23]. Thanks to the possibility to adjust laser parameters in real time during the LEE process, Wu et al. also demonstrated the possibility to obtain a gradient composition [24]. In addition, Dai et al. demonstrated the possibility to employ LEE also for the deposition of composites [25].

LAE, on the other side, does not use any external polarization and it only relies on the energy transferred by the laser to trigger the electrochemical reaction that leads to the formation of a layer of metal or alloy.

* Corresponding author.
E-mail address: roberto.bernasconi@polimi.it (R. Bernasconi).

https://doi.org/10.1016/j.surfcoat.2024.130849
Received 26 February 2024; Received in revised form 12 April 2024; Accepted 25 April 2024
Available online 26 April 2024

Table 1
Main specifications of the used laser system.

Parameter	Value
Wavelength, λ	532 nm
Max average power, $P_{avg,max}$	100 W
Pulse repetition rate, PRR	30 MHz
Pulse duration, τ	1.4 ns
Focal length, f_{foc}	260 mm
Waist diameter, d_0	38 μm

In the case of LAE, the energy barrier for deposition is higher than in LEE, but the substrate does not require any electrical connection with an external generator. From this point of view, LAE is characterized by a higher flexibility and scalability with respect to LEE. The technique has been used to deposit mainly Cu [26] and Au [27,28]. Laser induced metal reduction in absence of external polarization can also be performed on non-conductive substrates, provided that the solution is properly formulated [29–34]. This approach, similar to LAE, uses reducing agents to allow the reduction of metallic ions (similarly to electroless deposition). For what concerns LAE, no examples of deposition of alloys are available in literature.

Starting from this consideration, the present work aims at depositing for the first time a bicomponent metallic alloy using LAE. Palladium-platinum was selected as archetypical system to study the influence of bath formulation and laser parameters on the composition, morphology and physical properties of the deposited alloy. In particular, the manuscript tries to correlate the electrochemical properties of the electrolytes, determined using standard characterization techniques, with the properties of an alloy deposited with a non-standard technique like LAE. PdPt, besides being a significant model system for bimetallic alloys, can be potentially employed for aesthetic uses, for electrocatalytic applications [35] and for the electro oxidation of chemical species [36]. The latter reference employs a peculiar dealloying process for the production of PdPt, but PdPt can be obtained with more straightforward approaches like standard electrodeposition [37,38], electroless plating [39], nanoparticles coalescence [40], solvothermal synthesis [41] or sputtering [42]. However, considering that the most relevant features of LAE are its capability to deposit the material only on selected regions of the substrate and the possibility to get exceptionally high growth rates, the deposition of PdPt layers exploiting this technique is of particular interest.

2. Experimental methods

2.1. Laser setup

A nanosecond pulsed fiber laser source (Fig. S1) emitting at the second harmonic of 532 nm wavelength was used throughout the study (IPG GLPN-100-N, Cambridge, MA, USA). The laser source emitted 1.4 ns-long pulses at 30 MHz with a maximum average power of 100 W. The maximum peak power of the pulses was calculated as $P_{pk} = 2.4$ kW with a maximum pulse energy of $E = 3$ μJ. The wavelength of the laser allowed sufficient transmissivity with the employed electrolytes. The high average power provided a relatively higher deposition rate. The laser source was coupled to a galvanometric scanner to steer the beam with a 260 mm focusing lens and 38 μm spot diameter at the focal point (Superscan II, Raylase, Wessling, Germany). The main specifications of the system are reported in Table 1.

The laser beam was focused on the substrate inside the electrolyte tank. Deposition tests were carried out by scanning consecutive vector lines with a controlled hatch distance (H), laser power (P), scan speed (v), and the number of scanned layers (N). Within the different experimental campaigns, the power was varied between 5 and 30 W, the scan speed was varied between 0.1 and 2 mm/s, with up to 3 number of scanned layers. Hatch distance was maintained at 50 μm. The employed scan strategy was serpentine and the scan vectors were note rotated between the number of layers.

Table 2
Composition of the electrolytes employed.

	Pure Pd	Pure Pt	Pd 20 % at.	Pd 40 % at.	Pd 50 % at.	Pd 60 % at.	Pd 80 % at.
Platinum P salt	–	5 mM	4 mM	3 mM	2.5 mM	2 mM	1 mM
$PdCl_2$	5 mM	–	1 mM	2 mM	2.5 mM	3 mM	4 mM
$(NH_4)_2HPO_4$	100 g/L	100 g/L	100 g/L	100 g/L	100 g/L	100 g/L	100 g/L

The pH of all the solutions was corrected to 7 with NaOH.

2.2. Electrolytes

All the chemical employed during the deposition tests were acquired from Sigma Aldrich and used as received. The formulations of the different electrolytes are detailed in Table 2.

2.3. Electrochemical and LAE tests

All the deposition tests were carried out at room temperature on alpaca substrates coated with Ni (5 μm) and Au (500 nm). These were immersed in a glass tank containing the electrolyte, with about 1 mm of solution on top of the substrate (Fig. S2). The electrochemical characterization was performed using the C223AT screen-printed gold electrodes manufactured by DropSens. These were constituted by a gold working electrode (WE) of 1.6 mm of diameter, a gold counter electrode (CE) and a silver reference electrode (RE). More precisely, silver was used as pseudo-reference. The use of these disposable electrodes was required by the chronoamperometry (CA) tests performed under laser irradiation, which were performed placing a droplet of the solution under examination on the electrode and shining the laser on the WE. The WE was polarized at −200 mV or − 400 mV vs. Ag and the power of the laser P was progressively ramped from 5 to 20 W. The WE was exposed to the laser for 15 s at each power level (ON period), with brief periods without irradiation (OFF period). An Admiral Squidstat potentiostat/galvanostat was used to collect the data. In order to guarantee the best possible uniformity between the electrochemical measures, the use of the C223AT electrodes was extended also to the cyclic voltammetry (CV) characterization of the solutions. This was carried out immersing the electrodes in a beaker containing the solution under examination in a quiescent state.

2.4. Characterization techniques

The morphology of the deposited layers was studied by means of an EVO 50 EP scanning electron microscopy (SEM) setup, manufactured by Zeiss. The same microscope was equipped with a Model 7060 energy dispersive X-rays spectroscopy (EDS) module, manufactured by Oxford Instruments. The phase composition of the deposited films was analyzed using a X-rays diffraction (XRD) setup X-pert MPD setup produced by Philips, with Cu $K_{\alpha 1}$ radiation (1.5406 Å). The thickness of the layers was measured with a X-ray fluorescence (XRF) setup X-RAY XAN apparatus by Fischerscope. Atomic force microscopy (AFM) was carried out using a SOLVER PRO by NT-MDT (operated in contact mode). Finally, the hardness of the different alloys was determined by means of a Vickers microindenter HCV (by Fischerscope) equipped with a tip made of diamond. 30 mN was used as load force for all the indentation tests and this load was applied for 10 s.

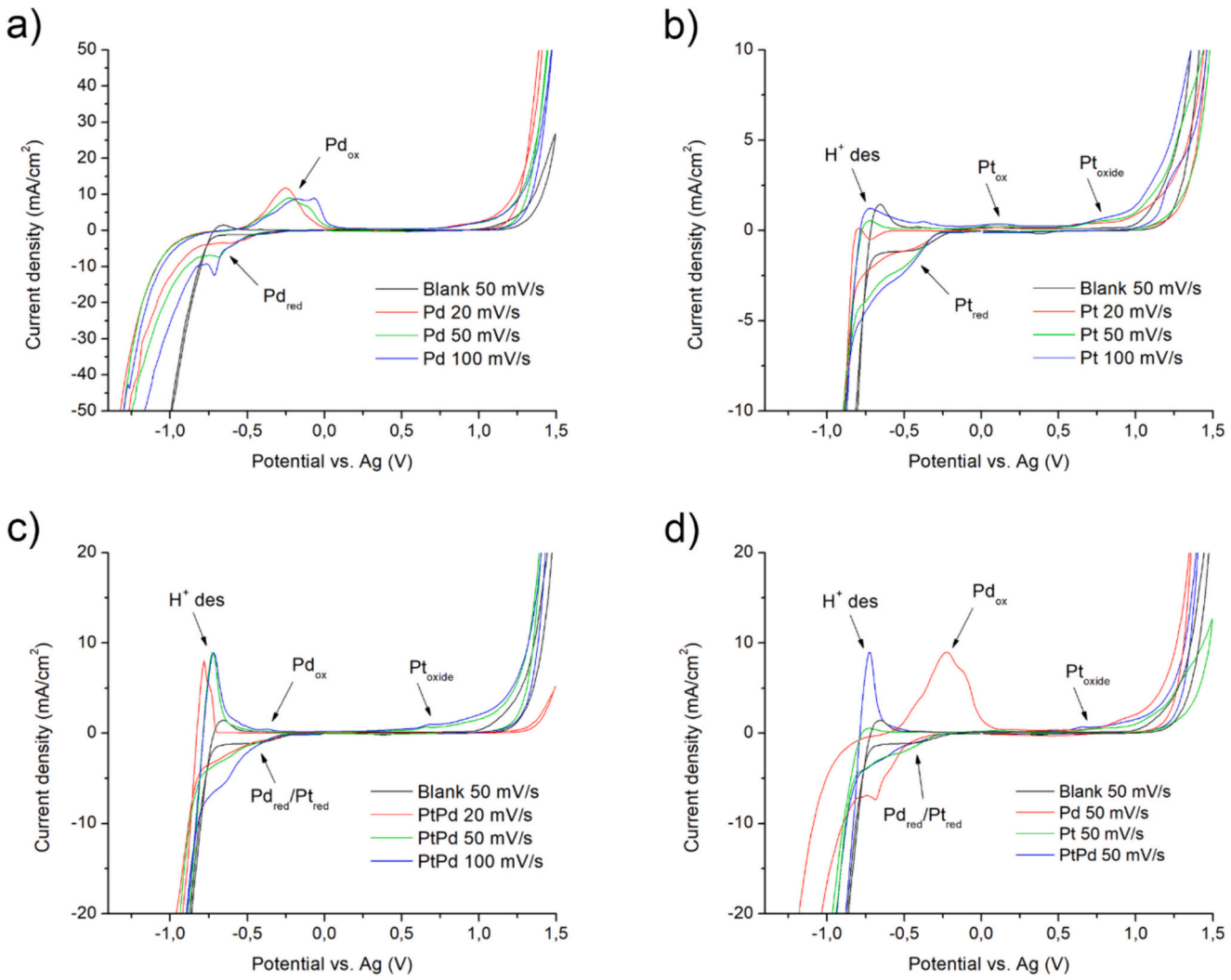

Fig. 1. CVs of the pure Pd electrolyte (a); CVs of the pure Pt electrolyte (b); CVs of the 50 % Pd electrolyte (c); comparison between the CVs acquired at 50 mV/s from the pure Pd, pure Pt and 50 % Pd electrolytes (d).

3. Results and discussion

3.1. Electrochemical characterization

As investigated by Puippe et al., the mechanism behind the deposition of metals under the influence of lasers is based on a shift in the rest potential in the zone irradiated as a consequence of a temperature variation at the metal-solution interface [13,15]. The verse and the extent of the shift depends on the nature of the metal being deposited. The condition for plating in the hot region illuminated by the laser is a positive shift of the rest potential. In this way, if the shift is enough to start the reduction of the metallic species in the electrolyte, the irradiated part behaves as a cathode and the surrounding zones as anode. On the contrary, if the shift is negative, dissolution occurs at the irradiated region and reduction on the neighboring annular zone. This effect justifies the occurrence of the redox reaction that leads to the deposition of the metal. In continuity with what discussed in the introduction, the potential gap required to start the reduction of the metal can be partially decreased by an external polarization (LEE) or totally filled by the laser alone (LAE). In addition, the presence of strong temperature gradients in correspondence of the zone hit by the laser also induces a strong microstirring and a considerable increase in charge transfer coefficients. These two contributions justify the very high plating rates typically observed in the case of LAE experiments.

If the mechanism presented by Puippe et al. is valid, this implies that the electroreduction of the Pd and Pt ions present in the electrolytes is purely based on a direct transfer of electrons. Therefore, in order to properly understand the results obtained, it was necessary to study and characterize the electrochemical behavior of the electrolytes (Figures from 1a to 1d). Fig. 1a reports the results obtained from the electrochemical characterization of the pure Pd electrolyte. The voltammogram of the solution containing only ammonium hydrogen phosphate (without the metal, identified as blank solution), is reported for comparison. In this reference CV, the only significant feature visible is a wave that starts at $E_{onset} - 210$ mV vs. Ag and that can be correlated with the electroreduction of the oxygen present in the electrolyte [43,44]. When Pd^{2+} ions are introduced in the electrolyte, the situation changes significantly. Regardless of the scan speed employed, two clear features can be identified [45]. The first, visible in the cathodic branch of the CV and marked as Pd_{red}, corresponds to the reduction of Pd^{2+} ions to Pd^0 and its E_{onset} is located at −322 mV vs. Ag. The second, visible in the anodic branch of the CV and identified as Pd_{ox}, corresponds to the oxidation of Pd^0 to Pd^{2+} and its peak potential E_{peak} is around −230 mV vs. Ag.

Fig. 1b shows the CVs obtained from the Pt containing electrolyte. In general, the situation represented in Fig. 1b corresponds to the deposition of Pt on gold (in the cathodic branch) and to the consequent anodic polarization of the resulting Pt layer during the reverse scan. Under this

Table 3
Electrochemical parameters (E_{onset} and i_{lim}) for the reduction of Pd and Pt alone or mixed in the same electrolyte.

	E_{onset}	i_{lim}	i_{lim} without blank
Blank electrolyte	−210 mV	−1.15 mA/cm^2	–
Pure Pd electrolyte	−322 mV	−7.07 mA/cm^2	−5.92 mA/cm^2
Pure Pt electrolyte	−272 mV	−2.26 mA/cm^2	−1.11 mA/cm^2
Pd 50 % at. electrolyte	−279 mV	−2.83 mA/cm^2	−1.68 mA/cm^2

conditions, Pt presents a wealth of typical features [46] and some of these are clearly visible in the picture. For what concerns the cathodic branch, the only relevant feature is the reduction of Pt^{2+} to metallic Pt at −272 mV vs. Ag (Pt_{red}). In the anodic region of the scan, however, three separate features are evident. The first one is the desorption of H^+ around −700 mV vs. Ag. The second and the third (Pt_{oxide}), located around 110 mV vs. Ag and 750 mV vs. Ag, are indicative of the formation of platinum oxide on the surface of the metal deposited during the cathodic scan.

For what concerns the alloy (Fig. 1c), a clear distinction between the reduction waves of the two metals cannot be observed due to the proximity of their E_{onset}. For this reason, the feature visible in the cathodic branch of the CV, with E_{onset} equal to −279 mV vs. Ag, is identified as Pt_{red}/Pd_{red}. The H+ desorption feature, at −700 mV vs. Ag in the anodic branch, is well developed, indicating a remarkable tendency of the alloy deposited during the cathodic scan to adsorb hydrogen. Due to the presence of Pt in the alloy, the formation of platinum oxide is evident also in this case (Pt_{oxide}).

By comparing the CVs obtained at 50 mV/s (Figs. 1d and S3), it is evident that the three electrochemical processes (Pd deposition, Pt deposition and PtPd plating) are characterized by comparatively similar E_{onset} but significantly different values of limiting current density (i_{lim}). It is possible to evaluate the limiting current densities for the reduction of the species present in the three different systems using the methodology described by Ponce de Leòn et al. [47], which is suitable for CVs where i_{lim} is not clearly visible. The results obtained are reported in Table 3, together with the E_{onset} values for the reduction of the metallic ions present in the three systems.

It is evident that Pd reduction from the electrolyte here employed is characterized by a limiting current considerably higher than the reduction of Pt. i_{lim} is linked to the mass transfer coefficient k through Eq. (1).

$$i_{lim} = -n\,F\,k\,C_0 \tag{1}$$

n is the number of electrons transferred (2 for both Pd^{2+} and Pt^{2+}), F is the Faraday constant and C_0 is the concentration of the reactant. Therefore, at the same ionic concentration, the mass transfer coefficient for Pd^{2+} reduction is considerably higher than the one typical of Pt^{2+} reduction. As expectable, the limiting current density of the alloy, resulting from the superimposition of the mass transfer coefficients of the two single metals, is in between the values observed for Pd and Pt.

The electrochemical characterization was completed by analyzing the effect of laser irradiation on the reduction process of the two metals, either alone or together in the electrolyte. To accomplish this task, CAs were carried out by placing a droplet of three different electrolytes (pure Pt, pure Pd and Pd 50 % at.) on the C223AT screen-printed gold electrodes. Then, the surface of the WE was exposed to the laser and the current flowing between the WE and the CE was measured. The WE was polarized at two distinct potentials: −200 and − 400 mV vs. Ag. These two potentials were selected considering the CV data obtained: at −200 mV vs. Ag, no reduction of any of the two metals takes place, while at −400 mV both metals reduce.

Initially, CAs were carried out on the electrolytes containing the pure metals (Figs. S4 and S5). By looking at the results obtained, it is evident that the laser induced a relevant variation in the current measured, regardless of the polarization potential applied. Obviously, the variation was more consistent at −400 mV vs. Ag, since at this potential the energy barrier to promote the movement of electrons is lower, and at high power levels. Nevertheless, a significant current was observed also at −200 mV vs. Ag (which is a potential that cannot alone induce the reduction of Pd or Pt). This is the condition typical of LEE. By comparing the behavior of Pt and Pd at a constant polarization of −400 mV vs. Ag

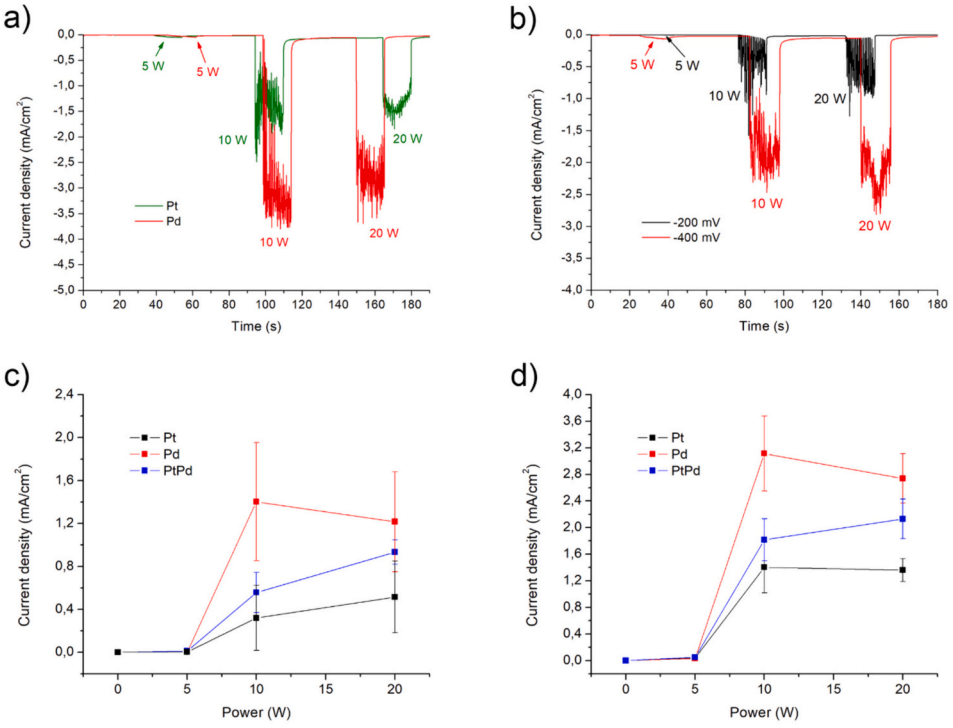

Fig. 2. Comparison between the CAs under laser irradiation for the pure Pd electrolyte and the pure Pt bath (a); CAs under laser irradiation for the 50 % Pd electrolyte (b); mean current levels measured during the ON time vs. laser power for the different electrolytes at −200 mV vs. Ag (c) and − 400 mV vs. Ag (d).

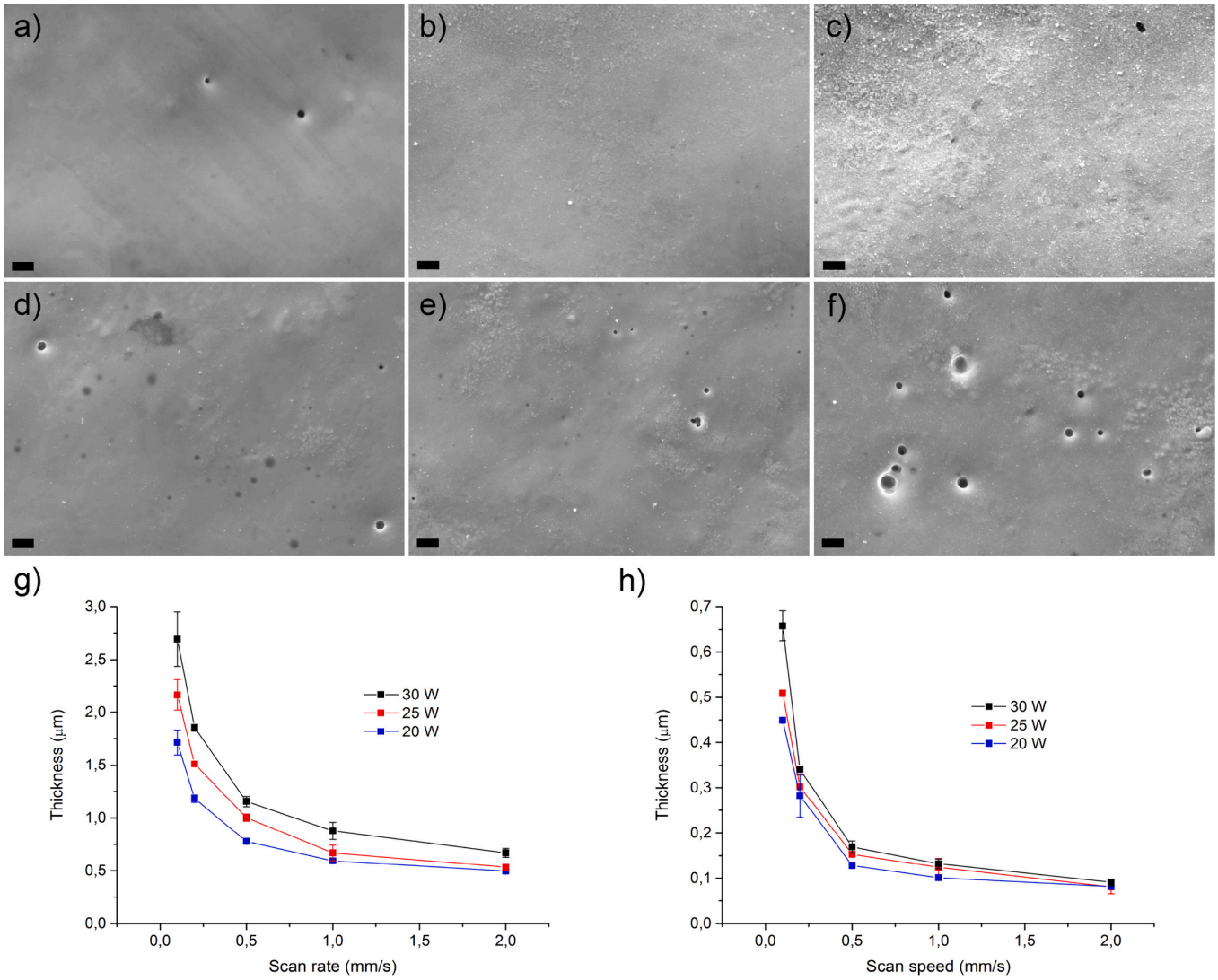

Fig. 3. SEM morphology of Pd layers deposited at 20 W (a), 25 W (b) and 30 W (c); SEM morphology of Pt layers deposited at 20 W (d), 25 W (e) and 30 W (f); thickness vs. v at different power levels for Pd deposition (g); thickness vs. v at different power levels for Pd deposition (h); all the scale bars correspond to 2 µm.

(Fig. 2a), it is evident that the currents observed in the case of Pt are lower than Pd. Due to the high reaction rates typical of LAE processes, it is reasonable to assume that the deposition process is under mass transfer control and that the currents observed during the tests are proportional to the limiting currents of the corresponding reduction reactions (in this case, the i_{lim} of Pt and Pd reduction). Pt presents a i_{lim} lower than Pd, and this explains the behavior visible in Fig. 2a.

A CA test was subsequently carried out also in presence of the 50 % at. Pd electrolyte, obtaining the result visible in Fig. 2b. Also in this case, the exposition to the laser radiation induced relevant currents, which are higher at the higher polarization potential and power levels. Some additional information can be obtained by evaluating the mean current registered during the ON periods at the three different power levels. The results obtained are reported in Fig. 2c (at −200 mV vs. Ag) and Fig. 2d (at −400 mV vs. Ag). As previously observed, the currents typical of Pd deposition are always higher than Pt. It is interesting to point out, however, that the currents observed in the case of the alloy are always in between the currents of the two pure metals. The reason for this behavior can be searched in the mixed potentials theory [48]. The global current for PdPt deposition (Eq. (2)) is the sum of the partial currents for Pd deposition (i_{Pd}), for Pt deposition (i_{Pt}) and for hydrogen evolution (i_{H2}).

$$i_{PdPt} = i_{Pd} + i_{Pt} + i_{H_2} \quad (2)$$

Considering that i_{Pd} is always larger than i_{Pt} at any given potential and that the limiting current density for Pd deposition is always larger than for Pd, it is not surprising that the current observed for PdPt deposition is the weighted sum of the two.

As final consideration, it is important to point out the effect of laser power. The values of current visible in Fig. 2c and d increase between 0 and 5 W and between 5 and 10 W, but are relatively stable between 10 and 20 W. This suggests that the current exchanged presents a plateau value at too high powers.

3.2. LAE deposition tests for pure Pd and Pt

Following the electrochemical characterization, the attention was focused on the deposition of continuous layers. Initially, the two pure metals were deposited separately. Figures from 3a to 3c show the SEM morphology of Pd layers deposited at v = 0.1 mm/s, H = 50 µm, $N = 1$ and increasing P levels. Figures from 3d to 3f show the SEM morphology of Pt layers deposited at v = 0.1 mm/s, H = 50 µm, N = 1 and increasing P levels. In general, the layers were characterized by a smooth surface, with Pd being characterized by a slightly rougher morphology at high P levels (Fig. 3c). In some cases, porosities were visible on the surface of

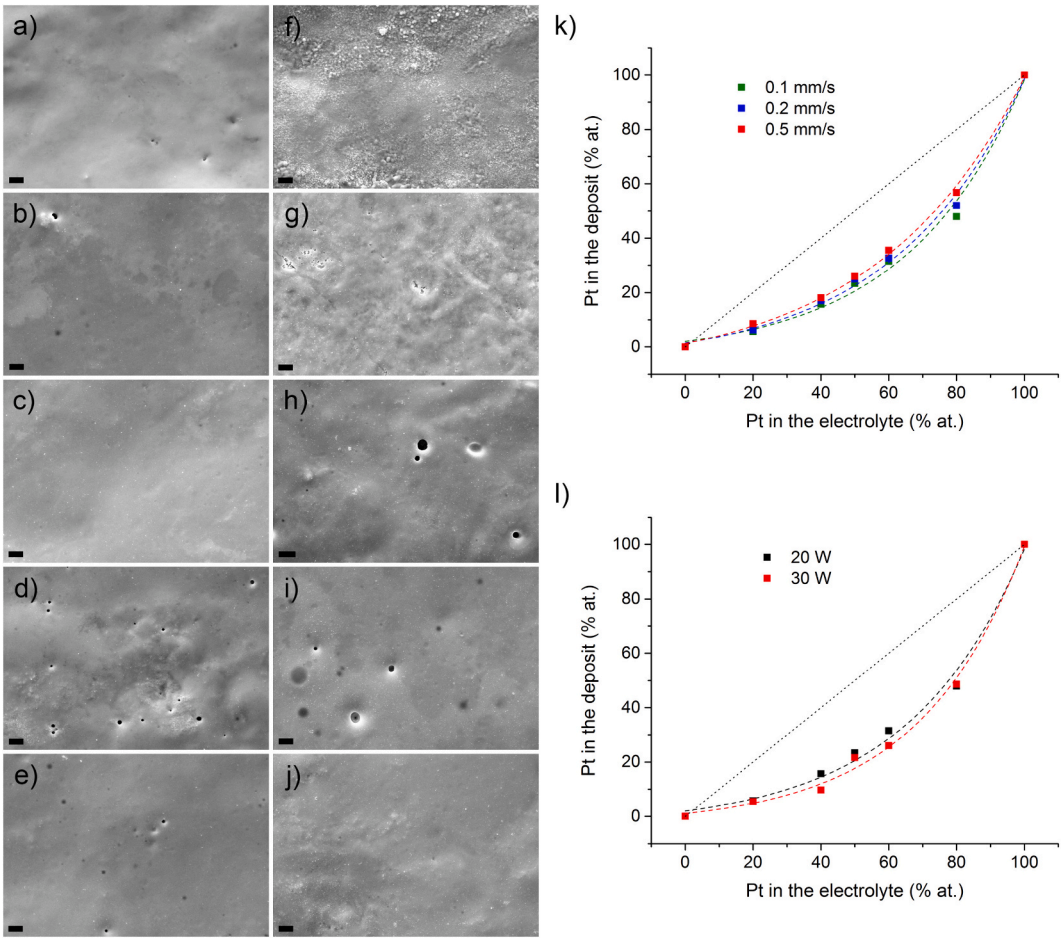

Fig. 4. SEM morphology of PdPt layers deposited from the 80 % Pd (a), 60 % Pd (b), 50 % Pd (c), 40 % Pd (d) and 20 % Pd (e) electrolytes at 20 W; SEM morphology of PdPt layers deposited from the 80 % Pd (f), 60 % Pd (g), 50 % Pd (h), 40 % Pd (i) and 20 % Pd (j) electrolytes at 30 W; Pt in the deposit vs. Pt in the electrolyte at different values of v with P = 30 W and H = 50 μm (k); Pt in the deposit vs. Pt in the electrolyte at different values of P with v = 0.1 mm/s and H = 50 μm (l); all the scalebars correspond to 2 μm.

the layers. The presence of pores is probably a result of gas evolution, either as hydrogen evolved during metal reduction or as vapor generated by water boiling in correspondence of the laser beam. From the chemical point of view (Figs. S6 and S7), the layers were relatively pure.

The thickness of the deposited layers as a function of v and P (at N = 1 and H = 50 μm), evaluated via XRF, is reported in Fig. 3g for Pd and in Fig. 3h for Pt. The growth rate of the two metals is proportional to the currents observed during the electrochemical tests (Fig. 2a) and, once again, to the limiting current densities measured during the CV tests (Table 3). Consequently, the thickness of the Pd layers was always higher with respect to the Pt coatings deposited under comparable conditions. Obviously, increasing power densities resulted in increased levels of thickness in the final layers. High scan speeds, on the contrary, decreased the amount of metal reduced (since the laser spot spends less time on each area of the pattern).

Regarding H and N, their effect was studied performing separate deposition tests. Fig. S8 shows the effect of an increasing number of scanned layers on the thickness of the resulting Pt layer (v = 0.5 mm/s, H = 50 μm, P = 30 W). As expectable, the thickness of the Pt layers increased linearly with N. The influence of H was verified performing two tests, at 50 μm and 25 μm (v = 0.5 mm/s, P = 30 W, N = 1). In the first case, the thickness of the Pt layer resulted equal to 0.169 μm, while in the second case it was equal to 0.351 μm (with a variation of +107.7 %).

One aspect that is worth mentioning is the minimum power of the laser required to induce appreciable deposition speeds and its correlation with the thermal properties of the substrate. The minimum level of P for the systems described in the present work was around 8 W. This value is considerably larger than the powers used in literature [13,26]. However, most of the available literature references deposit Cu, Ni or Au on thin metal layers sputtered on glass. In the present work, on the contrary, the metals have been deposited on bulk metallic substrates. As evidenced by Puippe et al. [13] and Von Gutfeld et al. [15], the growth rate of the LAE deposited metal presents a dependance on the thermal conductivity of the substrate. Indeed, highly conductive substrates (like the ones used here) efficiently dissipate the heat provided by the laser, making difficult the formation of large gradients of temperature between the cathodic and the anodic zone. Consequently, high laser powers are required to permit deposition. Glass, on the contrary, is characterized by a poor thermal conductivity. The thermal conductivity of a thin layer of metal deposited on glass is therefore much lower than a massive metal substrate. As a consequence, low power levels are sufficient to induce LAE.

3.3. LAE deposition tests for PdPt alloys

Since the LAE deposition of the two separate metals yielded positive results, the attention was subsequently moved to the deposition of compositionally controlled PdPt alloys. Figures from 4a to 4e show the SEM morphology of Pd layers deposited at v = 0.1 mm/s, H = 50 μm, P = 20 W and increasing Pt concentrations. Figures from 4f to 4j show the same but at P = 30 W. All the layers plated at the lowest power (20 W)

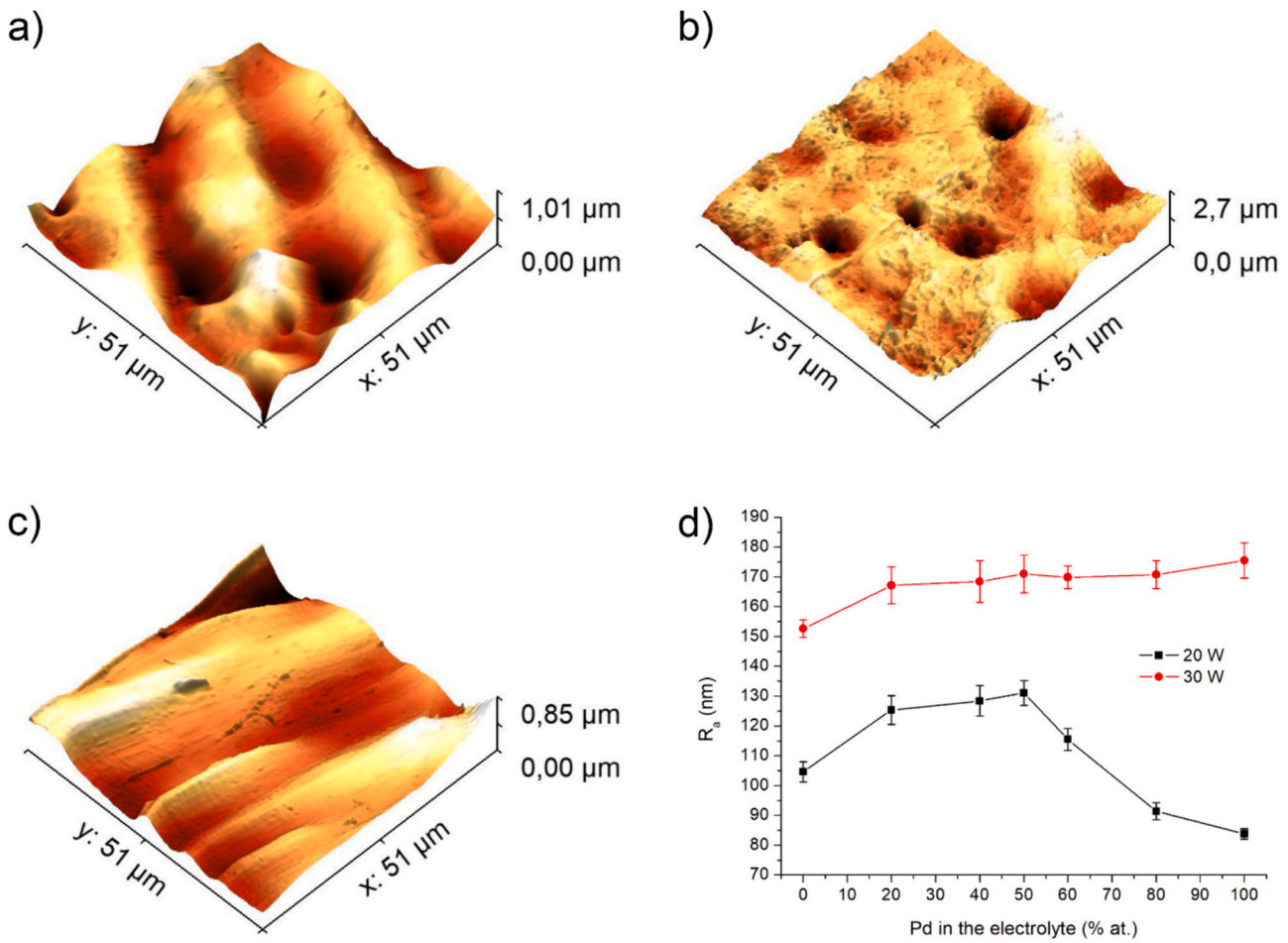

Fig. 5. AFM morphology of PdPt layers deposited from the 50 % Pd electrolyte at 20 W (a) and 30 W (b); AFM morphology of a PdPt layer deposited from the 80 % Pd electrolyte at 20 W (c); R_a data extracted from AFM for the PdPt layers analyzed.

were characterized by a relatively smooth, in some cases porous, morphology. The layers plated at 30 W, on the contrary, presented accentuated porosity and roughness levels. This is especially true at high Pd contents (Fig. 4f and g). From the chemical point of view (Figs. S9), the layers were relatively pure.

The composition of the layers as a function of Pt concentration in the electrolyte, scan rate v and power P was studied via EDS (Fig. 4k, l and S10). Due to its higher partial current density, resulting from its high i_{lim}, Pd codeposits preferentially in the alloy. All the alloys, therefore, are always Pd-rich with respect to the theoretical composition resulting from the electrolyte. Indeed, according to the mixed potentials theory, the composition of the alloy is proportional to the relative ratio between the partial currents of the two metals (Eq. (3)).

$$X_{Pd} = \frac{\frac{i_{Pd}}{n_{Pd}}}{\frac{i_{Pd}}{n_{Pd}} + \frac{i_{Pt}}{n_{Pt}}} \quad (3)$$

X_{Pd} is the molar fraction of Pd in the final alloy, while n_{Pd} and n_{Pt} are the number of exchanged electrons in the case of Pd and Pt reduction, respectively. Under the hypothesis of mass transfer control, the composition is therefore proportional to the i_{lim} of the metals. Consequently, Pd codeposits preferentially with respect to Pt and this effect can be observed also in standard electrodeposition processes, either in aqueous [49,50] and non-aqueous environment [51]. The composition of the electrolyte is the main factor influencing the final composition of the plated layers. P and v, conversely, have a limited influence. Apparently, high P levels and low v tend to increase the final Pd content of the alloy.

In addition to SEM, the morphology of the layers deposited was characterized also via AFM. Fig. 5a and b compare the morphology of the samples obtained from the 50 % Pd electrolyte at 20 W and 30 W, respectively (v = 0.1 mm/s, H = 50 µm). The layer obtained at the highest power is characterized by a rougher morphology, as already suggested by the SEM images (Fig. 4c and h). Fig. 5c shows the result obtained from the AFM characterization of a sample obtained from the 80 % Pd electrolyte at 20 W (v = 0.1 mm/s, H = 50 µm). If compared to the sample plated at the same power (Fig. 5a), the surface looks less rough. In order to be more quantitative, the R_a of the different samples was calculated from the AFM scans and represented in Fig. 5d (pure Pd and pure Pt are reported as well). As expected, the samples plated at higher power are rougher. At 20 W, the roughness present a peak in correspondence of the 50 % at. Pd composition of the bath. At 30 W, on the contrary, the highest roughness is measured on the pure Pd sample. This is consistent with the SEM characterization (Fig. 3c) and is probably connected to the high growth rate of Pd (at 30 W and 0.1 mm/s).

Obviously, also the thickness of the final alloy layer depends on the parameters employed and on the relative weight of the limiting current densities observed for the two metals. Fig. 6a reports the data obtained from the XRF characterization of the layers deposited from the two electrolytes containing the pure metals and from the electrolytes containing varying amounts of Pt and Pd. v was varied, while P was fixed at 30 W, N to 1 and H to 50 µm.

In analogy with the trends observed for the two metals, the thickness of the alloy layers decreases as the scan speed increases. In addition, the alloys present a trend connected to their composition: the thickness of the alloys is always comprised between the thickness of the Pd and Pt

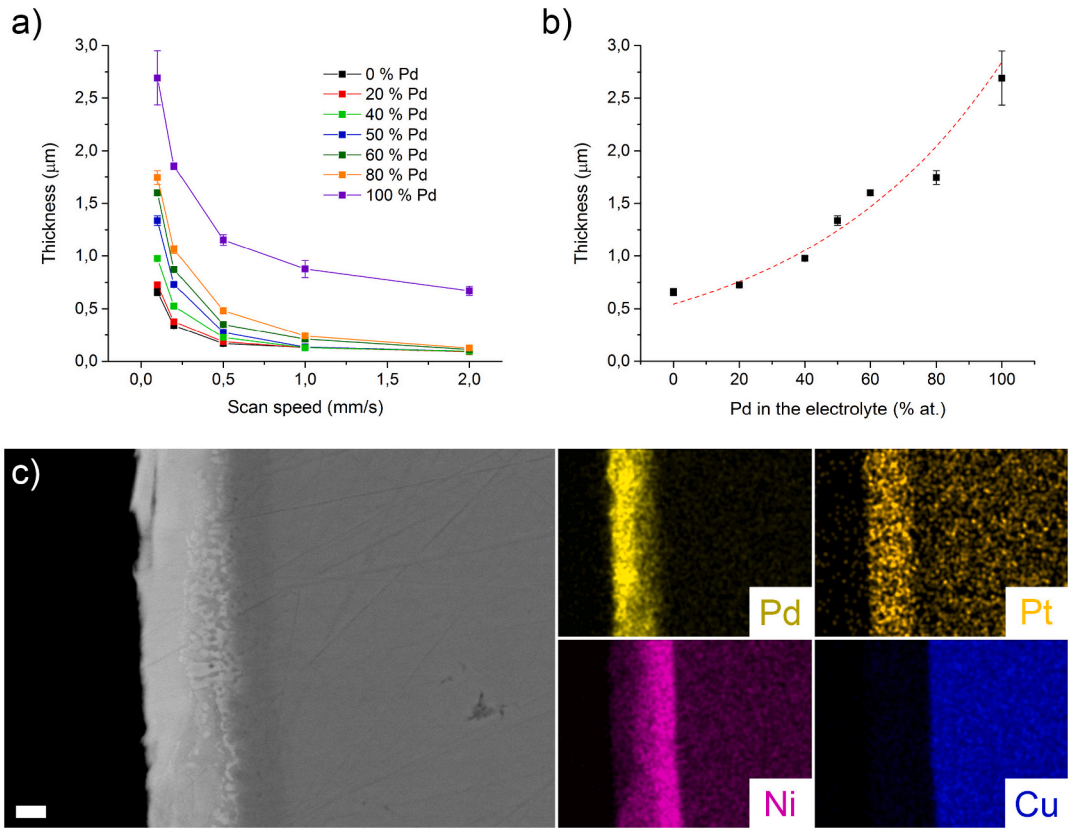

Fig. 6. Thickness vs. v for PdPt alloys deposited from different electrolytes with $P = 30$ W, $N = 1$, H = 50 μm (a); thickness vs. Pd in the electrolyte with v = 0.1 mm/s. (b); SEM morphology and EDS elemental mapping of the cross section of a PdPt layer deposited from the 50 % Pd electrolyte (c); the scalebar corresponds to 2 μm.

layers plated at the same parameters and it increases when the amount of Pd increases. This happens because the composition of the alloy is influenced by the partial current of the two metals (Eq. (3)). When the concentration of Pd in the bath increases, the weight of its partial current increases. Since it is higher than the partial current of Pt, it boosts the growth rate of the alloy. The effect can be visualized in a better way by plotting the thickness vs. relative percentage of Pd in the electrolyte at constant P (30 W) and v (0.1 mm/s), as visible in Fig. 6b.

Fig. 6c shows the cross section of a PtPd layer deposited at v = 0.1 mm/s, $P = 30$ W, $N = 1$, H = 50 μm from the 50 % at. Pd electrolyte. The morphological analysis is coupled with the EDS elemental mapping, which is reported in the four inserts on the right. By comparing the morphological and the compositional information, the presence of a 1.5–2 μm PdPt layer can be clearly observed. Some of the PdPt layer was dragged over the underlying Au and Ni layers during the polishing process. Nevertheless, the 5 μm Ni layer is still clearly visible. Due to its limited thickness, the Au layer has not been clearly detected. The Au signal, however, is still visible after the plating process (Figs. S6 and S7).

To conclude the characterization of the PdPt layers, their phase composition and hardness were characterized. The first was determined via XRD. If standard parameters are used to acquire the XRD spectra over a wide angular range (Fig. S11, P = 30 W, v = 0.1 mm/s, N = 1, H = 50 μm), no clear signs associated to the presence of Pt, Pd or PdPt can be observed. Indeed, the alpaca substrate and the two layers of Ni and Au yield a too strong signal, which hinders the signal connected to the presence of the deposited layers. The analysis was repeated decreasing the scan speed and limiting the angular range to 34.4° - 41° (Fig. 7a). This is the range were the (111) peaks for fcc Pd (JCPDS 05–0681) and fcc Pt (JCPDS 70–2057) are expected to be. The analysis evidenced, in the case of the two pure metals, the presence of the (111) peak in its expected position (40.196° for pure Pd and 39.946° for pure Pt). For what concerns the alloys, the (111) peak for the fcc phase was observed at varying angles. Pd and Pt, indeed, form a substitutional solid solution [52] and the position of the (111) peak is a function of the composition of the alloy [53,54]. The correlation between the Pt content of the alloy and the position of the (111) peak can be represented using the Vegard's law (Eq. (4)).

$$a_{PdPt} = X_{Pd}\, a_{Pd} + X_{Pt}\, a_{Pt} \tag{4}$$

The lattice parameter of the alloy a_{PdPt} correspond to the weighted mean between the lattice parameters of the two metals (a_{Pd} and a_{Pt}). Fig. 7b reports the value of a_{PdPt}, calculated from the position of the (111) peak, as a function of the Pt content of the alloy. As expectable from Eq. (4), the relationship between the atomic Pt content and a_{PdPt} is linear and indicative of the formation of a true substitutional solid solution between the two metals.

No quantitative information can be extracted from the full width at half maximum (FWHM), which is, unlike the position, negatively affected by the limited intensity of the peaks. In general, however, the peaks look broad and low in intensity, suggesting a nanocrystalline structure of the plated films. This is in line with the very high growth rates typical of LAE.

Hardness was evaluated via Vickers microindentation and the results of the tests are reported in Fig. 7c. In general, the hardness of the alloys is always lower than the pure metals. This may appear counterintuitive, as the alloy should present hardness levels higher than the two pure metals (due to solid solution strengthening). However, solid solution strengthening depends on the lattice strain induced by the solute. This is, in the case of Pd and Pt, very low as a consequence of the closely matching atomic radii of the two elements (137.6 pm vs. 138.5 pm). It is therefore probable that the solid solution strengthening is outweighed by the difference in crystallinity between the alloy and the pure metals. The pure metals are probably characterized by more refined grains, resulting in higher hardness levels.

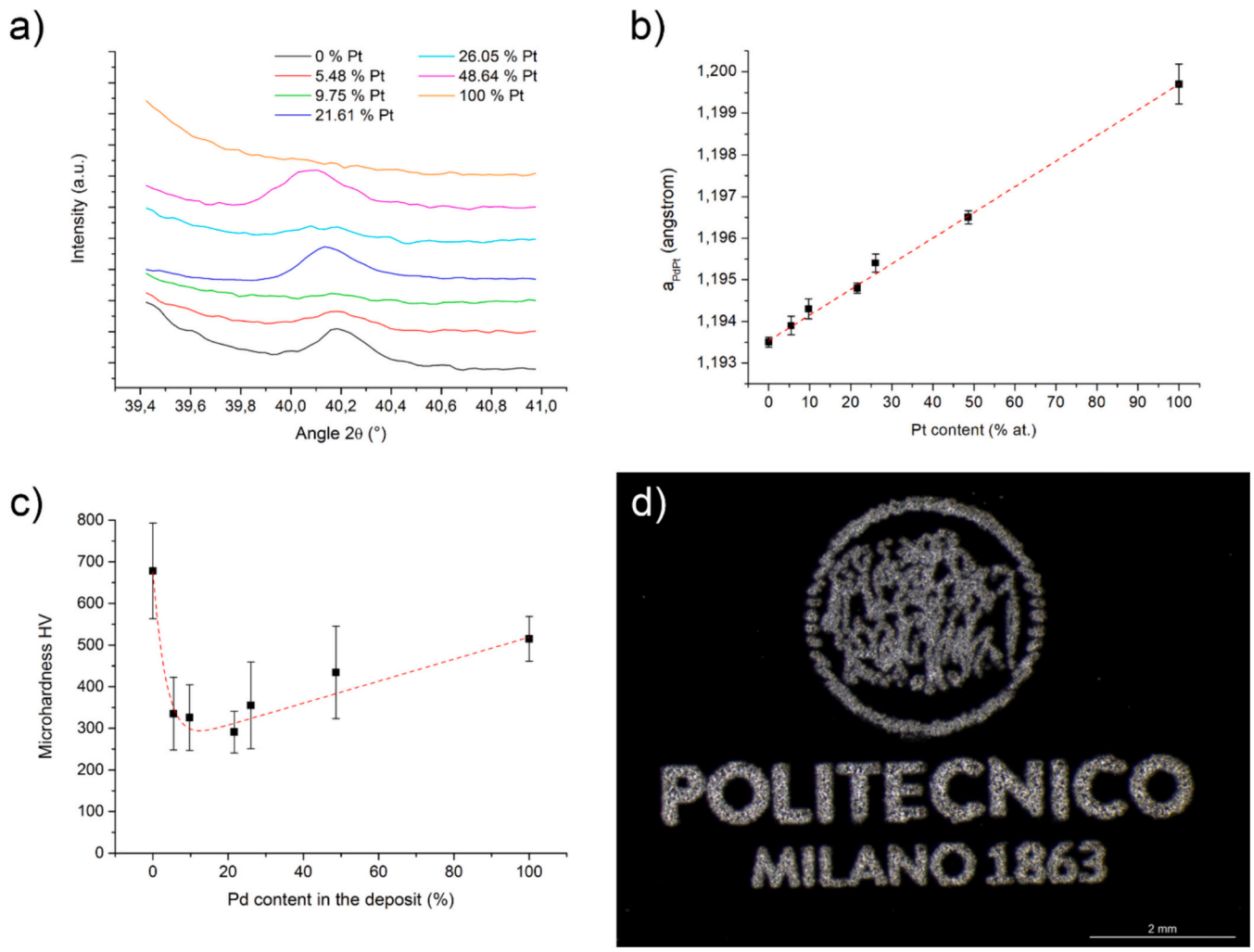

Fig. 7. XRD characterization of the layers deposited at $P = 30$ W, v = 0.1 mm/s, $N = 1$, H = 50 μm (a); lattice parameter for the (111) peak vs. Pt content of the alloys (b); microhardness vs. Pt content of the alloys (c); patterning test performed from the 50 % Pd electrolyte (d).

3.4. Patterning test

The main advantage of LAE with respect to other wet deposition techniques is the possibility to easily pattern the layers of metals obtained. This aspect was explored by depositing the PdPt alloy following a specific pattern. In particular, the laser was scanned to pattern the logo of Politecnico di Milano (the original bitmap employed is reported in Fig. S12, the result obtained is reported in Fig. 7d). The logo was deposited from the 50 % Pd electrolyte, employing the following parameters: v = 0.5 mm/s, P = 30 W, N = 1 and H = 50 μm. The material deposited under these conditions was characterized by a Pt content equal to 21.61 % at. (determined by EDS).

The LAE deposition test was successful and the general shape of the logo is clearly recognizable, but the resolution appears lower than the original bitmap. Moreover, some dimensions look altered along the scan direction. Fig. S13 reports a magnification of Fig. 7d, where these effects can be clearly observed. The letter O in the word "MILANO", for example, should be perfectly circular. On the contrary, its diameter was 630 μm along the x direction (d_x in Fig. S13) and 580 μm along the y direction (d_y in Fig. S13). Regarding the loss in resolution, it can be immediately verified by comparing the ratio between the width (w in Fig. S13) and the height (h in Fig. S13) of the number 1 present in the number "1863". Such ratio was 0.25, in front of a theoretical value of 0.154.

The two effects are related to the scan path followed by the laser, to the speed employed and to the diameter of the plated spot. These can be adjusted to improve the resolution of the deposition.

4. Conclusions

The experimental results obtained in the present work demonstrate the possibility to use laser assisted electrodeposition to plate alloys without any external polarization. In the case of PdPt deposition from an aqueous electrolyte, the energy provided by the laser promoted the reduction of Pd^{2+} and Pt^{2+} to form continuous layers of PdPt on gold. The composition of the layers was found to always be Pd-rich with respect to the composition of the corresponding electrolytes. This aspect was linked to the higher limiting current density detected for Pd^{2+} reduction. Under the reasonable assumption of mass controlled deposition, not only Pd preferentially deposited but also imparted high growth rates to Pd rich coatings as a consequence of its higher deposition current. The composition of the final alloy was found to primarily depend on the composition of the electrolyte rather than on the laser parameters. This aspect supports the assumption of a prevalently mass controlled process. In general, compositionally controllable layers of PdPt were successfully deposited. These were found to be nanostructured and characterized by a reduced degree of roughness. The material deposited showed the characteristics of a solid solution over the entire range of composition. In particular, the cell parameter for the (111) peak showed a linear variation with the Pt content of the alloy.

The hardness of the alloys was found to be always lower than the hardness of the two single metals, suggesting a limited influence of solid solution strengthening on the mechanical properties of the deposited materials. Finally, PdPt patterning was demonstrated by selectively plating the material in the form of a complex figure like the logo of Politecnico di Milano. The result obtained clearly shows the potential of LAE for the controlled patterning of alloys and supports its applicability for aesthetic or functional applications.

CRediT authorship contribution statement

Roberto Bernasconi: Writing – review & editing, Writing – original draft, Visualization, Methodology, Investigation, Formal analysis, Conceptualization. **Dario Crimella:** Validation, Methodology, Investigation, Data curation. **Ali Gökhan Demir:** Writing – original draft, Visualization, Software, Resources, Project administration. **Barbara Previtali:** Supervision, Software, Resources, Project administration. **Luca Magagnin:** Supervision, Software, Resources, Project administration.

Declaration of competing interest

The authors declare that they have no known competing financial interests or personal relationships that could have appeared to influence the work reported in this paper.

Data availability

Data will be made available on request.

Acknowledgements

The authors wish to express their gratitude to IPG Photonics for the longstanding collaboration. Raylase is gratefully acknowledged for the technical support provided. The authors also wish to thank Fabio Pagano for the AFM analysis of the samples.

Appendix A. Supplementary

Supplementary data to this article can be found online at https://doi.org/10.1016/j.surfcoat.2024.130849.

References

[1] P. Liu, Y. Liang, X. Lin, C. Wang, G. Yang, A general strategy to fabricate simple polyoxometalate nanostructures: electrochemistry-assisted laser ablation in liquid, ACS Nano 5 (2011) 4748–4755.
[2] V.A. Benderskii, A.V. Benderskii, Laser Electrochemistry of Intermediates, CRC Press, 1995.
[3] V.A. Benderskii, Laser electrochemistry of short-lived intermediate species, Electrochim. Acta 39 (1994) 1067–1074.
[4] I. Mandal, B. Doloi, State of the art on laser assisted electrochemical machining, in: IOP Conf. Ser. Mater. Sci. Eng, IOP Publishing, 2019, p. 12030.
[5] J. Song, Y. Liao, C. Liu, D. Lin, L. Qiao, Y. Cheng, K. Sugioka, K. Midorikawa, S. Zhang, Fabrication of gold microelectrodes on a glass substrate by femtosecond-laser-assisted electroless plating, J. Laser Micro Nanoeng. 7 (2012) 334–338, https://doi.org/10.2961/jlmn.2012.03.0018.
[6] R. Zhou, T. Huang, L. Chen, S. Chen, S. Lin, Y. Zhuo, Electroless deposition of confined copper layers based on selective activation by pulsed laser irradiation, J. Laser Micro Nanoeng. 12 (2017) 169–175, https://doi.org/10.2961/jlmn.2017.02.0021.
[7] M. Huske, J. Kickelhain, J. Muller, G. Eber, Laser supported activation and additive metallization of thermoplastics for 3D-MIDs, Proc. LANE. 3 (2001) 587–598. http://www.lpkfusa.com/articles/hdi/laser_activation.pdf.
[8] H.Y. Tsai, E. Ceretti, D. Rizzi, P. Ginestra, T.H. Kao, M.C. Leu, Laser induced metallization on flexible polymer coating: analysis and application, J. Mater. Process. Technol. 290 (2021), https://doi.org/10.1016/j.jmatprotec.2020.116986.
[9] A.G. Schrott, B. Braren, R. Saraf, Laser assisted Pd seeding for electroless plating on SiO2, Appl. Phys. Lett. 64 (1994) 1582–1584, https://doi.org/10.1063/1.111846.
[10] K. Ratautas, M. Andrulevičius, A. Jagminienė, I. Stankevičienė, E. Norkus, G. Račiukaitis, Laser-assisted selective copper deposition on commercial PA6 by catalytic electroless plating – process and activation mechanism, Appl. Surf. Sci. 470 (2019) 405–410, https://doi.org/10.1016/j.apsusc.2018.11.091.
[11] K. Ratautas, A. Jagminienė, I. Stankevičienė, M. Sadauskas, E. Norkus, G. Račiukaitis, Evaluation and optimisation of the SSAIL method for laser-assisted selective electroless copper deposition on dielectrics, Results Phys. 16 (2020), https://doi.org/10.1016/j.rinp.2020.102943.
[12] J. Ren, D. Li, Y. Zhang, W. Yang, H.Y. Nie, Y. Liu, Laser direct activation of polyimide for selective electroless plating of flexible conductive patterns, ACS Appl. Electron. Mater. (2022), https://doi.org/10.1021/acsaelm.1c01193.
[13] J.C. Puippe, R.E. Acosta, R.J. von Gutfeld, Investigation of laser-enhanced electroplating mechanisms, J. Electrochem. Soc. 128 (1981) 2539–2545, https://doi.org/10.1149/1.2127287.
[14] R.K. Gupta, A. Singh, A. Singh, P. Ram Sankar, S.K. Sharma, P.K. Mukhopadhyay, P. Ganesh, R. Kaul, K.S. Bindra, B. Singh, Maskless copper electroplating on stainless steel using DPSS green laser, Surf. Eng. 34 (2018) 446–453, https://doi.org/10.1080/02670844.2017.1396741.
[15] R.J. von Gutfeld, R.E. Acosta, L.T. Romankiw, Laser-enhanced plating and etching: mechanisms and applications, IBM J. Res. Dev. 26 (1982) 136–144, https://doi.org/10.1147/rd.262.0136.
[16] V.I. Grishko, W.W. Duley, Z.H. Gu, T.Z. Fahidy, Laser-assisted electrochemical deposition on certain cathodes, Electrochim. Acta 47 (2001) 643–650, https://doi.org/10.1016/S0013-4686(01)00779-4.
[17] R.J. Von Gutfeld, M.H. Gelchinski, D.R. Vigliotti, L.T. Romankiw, Laser-jet electrodeposition of gold and copper, in: Conf. Lasers Electro-Optics, Optica Publishing Group, 1984 p. THH3.
[18] I. Zouari, F. Lapicque, M. Calvo, M. Cabrera, Laser assisted metal electrodeposition: comprehensive investigation of zinc deposition, Chem. Eng. Sci. 45 (1990) 2467–2474, https://doi.org/10.1016/0009-2509(90)80130-7.
[19] Z. Zhang, Y. Wu, A. Wang, K. Xu, X. Dai, H. Zhu, S. Yang, A study on laser enhanced electrodeposition for preparation Fe-Ni alloy, Materials (Basel) 13 (2020), https://doi.org/10.3390/MA13163560.
[20] Y. Wu, Z. Zhang, K. Xu, J. Lu, A. Wang, X. Dai, H. Zhu, A study on the formation conditions of amorphous nickel-phosphorus (Ni-P) alloy by laser-assisted electrodeposition, Appl. Surf. Sci. 535 (2021) 147707, https://doi.org/10.1016/j.apsusc.2020.147707.
[21] Y. Wu, Z. Zhang, K. Xu, J. Lu, X. Dai, H. Zhu, S. Yang, Effect of laser single pulse energy on micro-structural, mechanical and corrosion properties of amorphous Ni-Fe-P alloy prepared by laser-assisted electrodeposition, Surfaces and Interfaces 22 (2021) 100811, https://doi.org/10.1016/j.surfin.2020.100811.
[22] Z. Zhang, Y. Wu, K. Xu, X. Dai, D. Zhao, H. Zhu, Y. Liu, A study on steady-state magnetic field in the surface morphology and internal stress of electrodeposited amorphous Ni-Fe-P alloy based on laser irradiation, Surf. Coatings Technol. 425 (2021) 127677, https://doi.org/10.1016/j.surfcoat.2021.127677.
[23] T. Ni, Z. Zhang, Y. Wu, S. Yang, Effects of laser energy on the surface quality and properties of electrodeposited zinc-nickel-molybdenum coatings, Nanotechnol. Precis. Eng. 6 (2023), https://doi.org/10.1063/10.0019382.
[24] Y. Wu, Z. Zhang, K. Xu, H. Zhu, Y. Liu, W. Lei, S. Yang, W. Shen, A novel strategy for designing Fe-Ni gradient multilayer coatings using laser-assisted electrodeposition and regulation mechanism, Surf. Coatings Technol. 452 (2023) 129088, https://doi.org/10.1016/j.surfcoat.2022.129088.
[25] X. Dai, K. Xu, Z. Zhang, L. Zhang, Y. Wu, H. Zhu, S. Yang, Study on Cu-Al2O3 metal-matrix composite coating prepared by laser-assisted electrodeposition, J. Electroanal. Chem. 904 (2022) 115855, https://doi.org/10.1016/j.jelechem.2021.115855.
[26] A.K. Al-Sufi, H.J. Eichler, J. Salk, H.J. Riedel, Laser induced copper plating, J. Appl. Phys. 54 (1983) 3629–3631, https://doi.org/10.1063/1.332404.
[27] H.R. Khan, M.U. Kittel, M.U. Kittel, S. Finishing, Laser-induced selective deposition on metal using electroless gold, NASF Surf. Technol. White Pap. 84 (2019) 6–13.
[28] A.K. de-Mesquita Braga, V. Baranauskas, A. Peled, Laser induced photodeposition of gold upon p-silicon immersed in chloroauric acid solutions, Appl. Surf. Sci. 79–80 (1994) 375–380, https://doi.org/10.1016/0169-4332(94)90439-1.
[29] G.A. Shafeev, Laser-assisted activation and metallization of polyimides, Appl. Phys. A Solids Surfaces. 55 (1992) 387–390, https://doi.org/10.1007/BF00324089.
[30] A. Manshina, A. Povolotskiy, T. Ivanova, A. Kurochkin, Y. Tver'yanovich, D. Kim, M. Kim, S.C. Kwon, Laser-assisted metal deposition from CuSO4-based electrolyte solution, Laser Phys. Lett. 4 (2007) 163–167, https://doi.org/10.1002/lapl.200610090.
[31] K. Kordás, J. Békési, R. Vajtai, L. Nánai, S. Leppävuori, A. Uusimäki, K. Bali, T. F. George, G. Galbács, F. Ignácz, P. Moilanen, Laser-assisted metal deposition from liquid-phase precursors on polymers, Appl. Surf. Sci. 172 (2001) 178–189, https://doi.org/10.1016/S0169-4332(00)00852-7.
[32] P. Rytlewski, B. Jagodziński, K. Moraczewski, Laser-assisted electroless metallization of polymer materials: a critical review, Rev. Adhes. Adhes. 4 (2016) 334–365, https://doi.org/10.7569/RAA.2016.097309.
[33] V.A. Kochemirovsky, M.Y. Skripkin, Y.S. Tveryanovich, A.S. Mereshchenko, A. O. Gorbunov, M.S. Panov, I.I. Tumkin, S.V. Safonov, Laser-induced copper deposition from aqueous and aqueous–organic solutions: state of the art and prospects of research, Russ. Chem. Rev. 84 (2015) 1059–1075, https://doi.org/10.1070/rcr4535.
[34] O.A. Lozhkina, M.S. Panov, L.S. Logunov, I.I. Tumkin, D.I. Gordeychuk, V. A. Kochemirovsky, Aluminum chloride reveals the catalytic activity towards laser-induced deposition of copper from water-based solutions, Int. J. Electrochem. Sci. 10 (2015) 6084–6091, https://doi.org/10.1016/s1452-3981(23)06704-4.
[35] M. Du, X. Li, H. Pang, Q. Xu, Alloy electrocatalysts, EnergyChem 5 (2023) 100083, https://doi.org/10.1016/j.enchem.2022.100083.

[36] C. Xu, Q. Hao, H. Duan, Nanoporous PdPt alloy as a highly active electrocatalyst for formic acid oxidation, J. Mater. Chem. A 2 (2014) 8875–8880.
[37] H. Wang, Y. Yamauchi, Synthesis of mesoporous platinum-palladium alloy films by electrochemical plating in aqueous surfactant solutions, Chem. - An Asian J. 7 (2012) 2133–2138, https://doi.org/10.1002/asia.201200316.
[38] J. Lu, S. Lu, D. Wang, M. Yang, Z. Liu, C. Xu, S.P. Jiang, Nano-structured PdxPt1-x/Ti anodes prepared by electrodeposition for alcohol electrooxidation, Electrochim. Acta 54 (2009) 5486–5491, https://doi.org/10.1016/j.electacta.2009.04.048.
[39] S.C. Lin, J.Y. Chen, Y.F. Hsieh, P.W. Wu, A facile route to prepare PdPt alloys for ethanol electro-oxidation in alkaline electrolyte, Mater. Lett. 65 (2011) 215–218, https://doi.org/10.1016/j.matlet.2010.10.006.
[40] C.Y. Cheng, Y.Y. Guo, Y.M. Zou, A.J. Ong, A.I.Y. Tok, S. Li, Melting mechanisms of Pt-based multimetallic spherical nanoparticles by molecular dynamics simulation, Rare Metals 42 (2023) 406–417, https://doi.org/10.1007/s12598-022-02160-5.
[41] Z.C. Zhang, J.F. Hui, Z.G. Guo, Q.Y. Yu, B. Xu, X. Zhang, Z.C. Liu, C.M. Xu, J. Sen Gao, X. Wang, Solvothermal synthesis of Pt-Pd alloys with selective shapes and their enhanced electrocatalytic activities, Nanoscale 4 (2012) 2633–2639, https://doi.org/10.1039/c2nr12135b.
[42] A. Caillard, S. Cuynet, T. Lecas, P. Andreazza, M. Mikikian, A.L. Thomann, P. Brault, PdPt catalyst synthesized using a gas aggregation source and magnetron sputtering for fuel cell electrodes, J. Phys. D Appl. Phys. 48 (2015), https://doi.org/10.1088/0022-3727/48/47/475302.
[43] Y. Guo, M. Yang, R.C. Xie, R.G. Compton, The oxygen reduction reaction at silver electrodes in high chloride media and the implications for silver nanoparticle toxicity, Chem. Sci. 12 (2021) 397–406, https://doi.org/10.1039/d0sc04295a.
[44] A.C. Bakir, N. Ahin, R. Polat, Z. Dursun, Electrocatalytic reduction of oxygen on bimetallic copper-gold nanoparticles-multiwalled carbon nanotube modified glassy carbon electrode in alkaline solution, J. Electroanal. Chem. 662 (2011) 275–280, https://doi.org/10.1016/j.jelechem.2011.06.016.
[45] M. Asnavandi, B.H.R. Suryanto, C. Zhao, Controlled electrodeposition of nanostructured Pd thin films from protic ionic liquids for electrocatalytic oxygen reduction reactions, RSC Adv. 5 (2015) 74017–74023, https://doi.org/10.1039/c5ra13898a.
[46] D.W. Kumsa, N. Bhadra, E.M. Hudak, S.C. Kelley, D.F. Untereker, J.T. Mortimer, Electron transfer processes occurring on platinum neural stimulating electrodes: a tutorial on the i(V e) profile, J. Neural Eng. 13 (2016) 1–15, https://doi.org/10.1088/1741-2560/13/5/052001.
[47] C. Ponce-De-León, R.W. Field, On the determination of limiting current density from uncertain data, J. Appl. Electrochem. 30 (2000) 1087–1090, https://doi.org/10.1023/A:1004015617522.
[48] D. Landolt, Fundamental aspects of alloy plating, Plat. Surf. Finish. 88 (2001) 70–79.
[49] S. Guerin, G.S. Attard, Electrochemical behaviour of electrodeposited nanostructured palladium + platinum films in 2 M H2SO4, Electrochem. Commun. 3 (2001) 544–548, https://doi.org/10.1016/S1388-2481(01)00211-9.
[50] X. Quan, Y. Mei, H. Xu, B. Sun, X. Zhang, Optimization of Pt-Pd alloy catalyst and supporting materials for oxygen reduction in air-cathode microbial fuel cells, Electrochim. Acta 165 (2015) 72–77, https://doi.org/10.1016/j.electacta.2015.02.235.
[51] M. Manolova, R. Böck, I. Scharf, T. Mehner, T. Lampke, Electrodeposition of Pd alloys from choline chloride/urea deep eutectic solvents, J. Alloys Compd. 855 (2021), https://doi.org/10.1016/j.jallcom.2020.157462.S.
[52] S.R. Bharadwaj, A.S. Kerkar, S.N. Tripathi, S.R. Dharwadkar, The palladium-platinum phase diagram, J. Less-Common Met. 169 (1991) 167–172, https://doi.org/10.1016/0022-5088(91)90245-Y.
[53] C.A. Rodríguez-Proenza, J.P. Palomares-Báez, M.A. Chávez-Rojo, A.F. García-Ruiz, C.L. Azanza-Ricardo, A. Santoveña-Uribe, G. Luna-Bárcenas, J.L. Rodríguez-López, R. Esparza, Atomic surface segregation and structural characterization of PdPt bimetallic nanoparticles, Materials (Basel) 11 (2018) 1–15, https://doi.org/10.3390/ma11101882.
[54] L. Bindi, F. Zaccarini, G. Garuti, N. Angeli, The solid solution between platinum and palladium in nature, Mineral. Mag. 77 (2013) 269–274, https://doi.org/10.1180/minmag.2013.077.3.04.